Title

Microstructural abnormalities are evident by histology but not HR-pQCT at the periosteal cortex of the human tibia under CVD and T2D conditions

Authors

Garita, Barbara
Maligro, Jenna
Sadoughi, Saghi
et al.

Publication Date

2021-06-01

DOI

10.1016/j.medntd.2021.100062

HHS Public Access

Author manuscript

Med Nov Technol Devices. Author manuscript; available in PMC 2023 June 28.

Published in final edited form as:

Med Nov Technol Devices. 2021 June ; 10: . doi:10.1016/j.medntd.2021.100062.

Microstructural abnormalities are evident by histology but not HR-pQCT at the periosteal cortex of the human tibia under CVD and T2D conditions

Barbara Garita[a], **Jenna Maligro**[a], **Saghi Sadoughi**[a], **Po Hung Wu**[a], **Ellen Liebenberg**[b], **Andrew Horvai**[c], **Thomas M. Link**[a], **Galateia J. Kazakia**[a,*]

[a]Department of Radiology and Biomedical Imaging, University of California, San Francisco, 185 Berry St Suite 350, San Francisco, CA, 94107, USA

[b]Department of Orthopaedic Surgery, University of California, San Francisco, 513 Parnassus Avenue, San Francisco, CA, 94143, USA

[c]Department of Pathology, University of California, San Francisco, 1825 4th St, San Francisco, CA, 94143, USA

Abstract

Cortical bone microstructure deficits may increase fracture risk in individuals with cardiovascular disease and diabetes. High resolution peripheral quantitative computed tomography (HR-pQCT) enables in vivo microstructure characterization but is limited in its ability to visualize important biological features. We conducted histological analyses and HR-pQCT imaging of distal tibia bone samples from 6 donors with cardiovascular disease (CVD) and type 2 diabetes mellitus (T2D). Histology but not HR-pQCT identified previously undocumented morphopathological deficits that may contribute to cortical bone fragility. These observations may provide guidance for improved HR-pQCT microstructural characterization as well as insight into mechanisms of cortical bone degradation.

Keywords

Cortical bone porosity; Type 2 diabetes; HR-pQCT

1. Introduction

In the last decade, high resolution peripheral quantitative computed tomography (HR-pQCT) has been used to evaluate in vivo changes in bone morphology resulting from agingand disease-related bone loss [1–3]. This technology is a step forward from conventional bone density assessment with Dual-energy X-ray Absorptiometry (DXA). In contrast to DXA, HR-pQCT provides three-dimensional assessment of cortical and trabecular macrostructure

*Corresponding author. galateia.kazakia@ucsf.edu (G.J. Kazakia).

Declaration of competing interest

The authors declare that there are no conflicts of interest.

and microstructure captured at resolutions on the order of 100 μm. One important example of the use of this technology is the investigation of structural changes underlying increased bone fracture risk in individuals with type 2 diabetes mellitus (T2D). This has been particularly impactful because bone mineral density (BMD) measurements obtained via DXA have underpredicted the risk of bone fracture in individuals with T2D [4]. Research findings based on data obtained using HR-pQCT, on the other hand, have shown that increased cortical porosity of diabetic bone is associated with the high risk of fragility fractures [5,6]. Subsequent HR-pQCT analyses investigating co-morbidities have identified T2D patients with a history of fragility fractures [3,7] and microvascular complications [8] as subgroups particularly impacted by cortical microstructure deficits. HR-pQCT has also been used to investigate trabecular and cortical microstructure in the context of cardiovascular disease [9,10]. HR-pQCT was found to be reliable in simultaneously evaluating arterial calcification and bone microstructural characteristics [9], finding an association between increased arterial calcification and deficits in cortical microstructure [11].

While HR-pQCT enables visualization of bone microstructure at resolutions unmatched by other existing imaging modalities, it is limited in its ability to visualize important biological features. HR-pQCT can detect large cortical pores but cannot visualize bone features smaller than ~100 μm, such as smaller pores, canals, lacunae, and canaliculi. Further, as an in vivo x-ray based technology, HR-pQCT cannot detect or characterize cellular or extracellular organic components. Compromised extracellular matrix properties play a causal role in bone fragility [12,13]. Recently, Dole et al. showed that microstructural alterations at the length-scale of the perilacunar/canalicular network can cause severe bone fragility, even when bone mass and macro-scale features are unaffected [14]. Therefore, while HR-pQCT is a powerful in vivo imaging tool, it is insufficient to capture important microstructural deficits and related cellular processes that can affect bone formation, remodeling, and tissue-level mechanical properties. Histological evaluation of post-mortem samples can be used to fill this gap in knowledge and aid in interpretation of features visualized via in vivo HR-pQCT.

The goal of this observational study, given the potentially important role that cortical bone microstructural changes may have in mediating bone fracture risk in individuals with T2D and CVD, and the known limitations of HR-pQCT, was to evaluate cortical bone microstructural abnormalities in samples obtained from individuals with CVD and T2D using histological techniques. We prepared histological sections from bone samples obtained from six different individuals with CVD, including individuals with both CVD and T2D. We identified previously unreported microstructural abnormalities visualized in these histological sections and assessed the capability of HR-pQCT to detect these microstructural features. To our knowledge, these microstructural deficits have not been documented or described previously, but may be important in the interpretation of HR-pQCT findings and contribute to the understanding of bone fracture risk in the setting of CVD and T2D.

2. Methods

2.1. Sample acquisition and preparation

UCSF institutional review board approval was obtained prior to the start of the study. We performed a histological analysis of six human distal tibia sections obtained from elderly donors (mean age 79 years) with cardiovascular disease (CVD), three of whom also had type 2 diabetes (T2D) for a duration of 10 years or more (Table 1). All three of the CVD-only cases were osteoporotic and had previous fragility fractures. Full tibia specimens were collected from cadaver donors (National Disease Research Interchange and Life Legacy Foundation). Tibia specimens were collected within 24 h of death, stripped of soft tissues and wrapped in saline-soaked underpads, and maintained at 4 °C starting at the time of harvest and continuously until fixation. One 4-cm long axial segment, incorporating the standard in vivo HR-pQCT imaging site, was sectioned from the distal end of each tibia by cutting at 22 mm and 62 mm distance from the articular surface. Each segment was sealed in parafilm and encased in a cube of polymer foam (PolyFoam® Polytek) to aid in consistent positioning for the following steps.

2.2. HR-pQCT image acquisition and processing

Prepared specimens were imaged using HR-pQCT (XtremeCT, Scanco Medical AG). Image data was acquired with scan settings of 60 kVp source potential and 900 μA tube current, recording 1000 projections at 300 ms integration time per projection. The 12.6 cm field of view (FOV) was reconstructed across a 3072 × 3072 matrix, yielding three-dimensional image volumes comprised of 41 μm isotropic voxels (88 μm true spatial resolution as measured by 10% modulation transfer function MTF [15]). The axial length imaged was 9.02 mm, positioned at the standard in vivo ultra-distal tibia imaging site. HR-pQCT image data were down-sampled to produce a second set of scans at 82 μm voxel size (128 μm true spatial resolution [15]). Both image sets were processed to determine cortical bone boundaries using established, semi-automated HR-pQCT image analysis techniques. Specifically, the 82 μm images were contoured using the manufacturer's standard algorithms [16,17]. The 41 μm images were contoured using the same algorithms with parameters optimized for 41 μm data, as described in detail in previous publications [15,18].

2.3. Histology processing

Following HR-pQCT image acquisition, 4 slabs (each 5 mm thick) were cut from each foam-embedded segment using a band saw and fixed in 10% neutral buffered formalin. Slabs were decalcified using an ionexchange decalcifying unit (Biocare Medical, Concord, CA). After decalcification, slabs were dehydrated in progressive concentrations of ethanol and paraffin embedded. From these slabs, 5 μm thick sections were cut, mounted, and stained with hematoxylin and eosin, and adjacent sections were stained with Heidenhain connective tissue stain containing aniline blue, orange G, and acid fuchsin. High resolution full cross-section images of the stained tibia sections were created by capturing 5x and 20x images on a digital microscope and tiling them into a whole slide histology image (Fig. 1).

2.4. Matching of histology to HR-pQCT images

Histology and HR-pQCT images were pre-aligned using orientation markings and distance measurements on the foam blocks encasing the embedded tibia segments. Once histology sections were processed, final alignment was performed manually by comparing cortical and trabecular structures between HR-pQCT and histology images.

3. Results

3.1. Subperiosteal circumferential porosity

Large, sub-periosteal pores running circumferentially along the outer cortex were observed in all histological images of all six tibia samples (Fig. 2). These circumferential pores contained primarily adipocytes, with evidence of vessels, capillaries, and connective fibrous tissue. In contrast, typical osteonal pore space (also evident in Fig. 2) contained primarily vascular and neuronal structures with surrounding connective fibrous tissue anchoring vessels to canal walls. Evidence of tunneling was observed within the circumferential pores, including osteoclasts and scalloping of the bone surface (Fig. 2 G and H). These circumferential pores did not appear to be connected to the marrow space, based on histological and HR-pQCT image visualization. In a subset of circumferential pores, pore space appeared to be connected to the periosteal surface. In others, a thin outer woven bone layer encapsulated the pore and separated pore space from the periosteum. When viewed under polarized light, this woven bone layer was observed to be composed of short haphazardly arranged collagen fibrils of diminished birefringence (Fig. 3). These sub-periosteal circumferential pores were located within approximately 300 μm of the periosteal surface. They extended circumferentially from 400 μm to 7 mm in length, with a width of approximately 150–200 μm. Axially, these circumferential pores extended up to 9 mm along the long axis of the tibia, as measured in consecutive slices on 3D HR-pQCT reconstructions.

3.2. Irregular bone-periosteum interface

In all cadaver samples analyzed, large sections of the periosteal cortical boundary lacked organized circumferential lamellae. The periosteum-bone surface interface was frequently convoluted. Under polarized light small sections of outer lamellae were interrupted by an irregular cortex composed of eroded cavities and circumferential pores. In place of organized lamellar collagen fibers there were short, disorganized fibers presenting with less birefringence when visualized under polarized light, suggestive of woven bone (Fig. 3).

3.3. Periosteal bone matrix deterioration

In specimens from donors with both CVD and T2D, but not those from donors with CVD alone, we observed sites of bone matrix disintegration surrounding and in proximity to osteocyte lacunae in the sub-periosteal cortex (Fig. 4). These sites of disintegration were seen only in the zone closest to the periosteum, often between the circumferential pores and the periosteal border, not in any other areas of the cortex. The majority of lacunae within and around the zones of matrix disintegration contained visible osteocyte nuclei, indicating these zones were not osteonecrotic. Polarized light microscopy revealed loss of

lamellar organization within zones of bone matrix deterioration, with reduced birefringence and short, disorganized fibers.

3.4. HR-pQCT visualization of cortical features

Visualization of circumferential pores by HR-pQCT depended on the resolution of HR-pQCT and the proximity of pores to the periosteal surface. Images at 41 μm voxel size captured more of the circumferential pores than images at 82 μm voxel size. Circumferential pores in close proximity to the periosteal surface (less than 100 μm) were not visualized at either resolution. Circumferential pores situated between 150 and 200 μm from the periosteal surface were identifiable with HR-pQCT at both resolutions. In most cases, with the exception of pores located further from the periosteum, the automated periosteal contour resulting from standard image processing excluded the circumferential pores (Fig. 5). These excluded circumferential pores would not be considered in any subsequent image processing and morphological quantification.

4. Discussion

In this study, we reported on previously unidentified microstructural deficits in the outer cortex of the human distal tibia from donors with CVD and T2D. We identified the presence of predominately adipocyte-filled circumferential pores in the sub-periosteal cortex in all samples analyzed. The location, unusual morphology, and adipocyte content of these pores were the major characteristics of these pathological findings. These circumferential pores are not normal Haversian or Volkmann Canals; their long axis runs circumferentially along the outer cortex extending up to 7 mm in length. Some circumferential pores did contain longitudinally oriented vessels; therefore, we cannot exclude the possibility that they represent the residuum of Haversian canals that have coalesced. In all samples, large sections of the periosteal surface lacked an organized outer lamellar layer and rather were composed of disorganized woven fibrils. In samples from donors with both CVD and T2D, but not from those with CVD alone, zones of bone matrix degradation, characterized by small foci of tissue disintegration, were apparent in proximity to the sub-periosteal circumferential pores. To the best of our knowledge these features have not previously been reported; however, they can provide insight into the impact of disease on bone biology, bone quality, and fracture risk.

Sub-periosteal circumferential pores have not been identified in previous HR-pQCT studies of the distal tibia. Our own studies have focused on detailed spatial analysis of cortical pore location, including the quantification of pore distribution throughout quadrants and across lamellar layers [19,20] of the cortex. These studies documented that spatial analysis of pore distribution increases sensitivity of microstructural and biomechanical analyses and improves understanding of biological mechanisms and outcomes of disease [1,19,21]. However, these detailed HR-pQCT-based analyses of pore distribution did not detect the sub-periosteal circumferential pores described here. There are a number of reasons that they may have gone undetected, including limited spatial resolution, limitations in the standard automated image processing routines, and a lack of coordinated histological analyses. HR-pQCT is operating in a resolution-limited regime where partial volume effects can

obscure small microstructural features. In the case of these circumferential pores, though the pores themselves are large relative to HR-pQCT resolution, the surrounding structures, in particular the periosteal borders, are fine and often obscured on HR-pQCT. The thin border, possibly combined with low mineralization, produces low attenuation on HR-pQCT, which is then eliminated by the automated periosteal contouring and post-processing routines. Exclusion of these pores in standard HR-pQCT analysis will have implications in the quantitative results, including underestimation of porosity and cortical thickness, and misrepresentation of pore size, morphology, and spatial distribution. On closer inspection and re-analysis of in vivo patient scans in a T2D cohort, we have been able to identify and include these sub-periosteal circumferential pores by manually adjusting the periosteal boundary during image processing. The quantitative impact of this adjustment is the subject of ongoing work and will be addressed in a future publication.

In the present study, we report long sub-periosteal circumferential pores predominantly filled with adipocytes, disorganized periosteal lamellae, and foci of bone matrix disintegration adjacent to the periosteal border in samples from donors with both CVD and T2D. These observations represent microstructural changes that result in poor bone quality and may contribute to increased fracture risk, but which have not been observed before because of a lack of histological studies on bone from donors with CVD and T2D [22,23]. In CVD and T2D, collagen glycosylation, cytokine mediated pro-inflammatory states, and oxidative stress effects impact bone quality [24]. At the level of the osteon, these processes may lead to changes in collagen fiber size and orientation [25], peri-canalicular resorption [26], osteocyte death [27] and changes in the periosteum [28]. While our results underscore the importance of histological validation and confirm that standard HR-pQCT analysis techniques are insufficient to capture important microstructural deficits related to cellular processes that affect bone remodeling and formation, our observations may aid HR-pQCT researchers attempting to capture more structural detail at the periosteal border. In light of the recent release of a new generation HR-pQCT with increased spatial resolution and improved processing techniques, improved accuracy in microstructural quantification of circumferential porosity may be achievable.

The sub-periosteal circumferential pores may have developed secondary to irregular periosteal apposition or due to osteoclast-driven resorption and tunneling. Our observations of the presence of osteoclasts within the circumferential pores, coupled with periosteal bone morphology inconsistent with apposition, lead us to believe that these pores are resorptive rather than forming secondary to periosteal apposition. More studies will be necessary to confirm this conclusion. Prospective in vivo studies using HR-pQCT combined with precise spatial image registration to visualize specific areas of bone formation and resorption in time-lapse HR-pQCT [29] may also be helpful in determining whether periosteal apposition or resorptive tunneling is creating these sub-periosteal pores. Using the highest resolution new generation HR-pQCT scanner and incorporating the approach, developed through this work, of manually adjusting the periosteal contour, time-lapse HR-pQCT may have the potential to categorize individual voxels within and surrounding sub-periosteal circumferential pores as formed or removed over the follow up period.

The content of the sub-periosteal circumferential pores can give some insight into the biological mechanisms driving their development. The presence of vessels and capillaries in these circumferential pores may indicate the expansion of the vascular network with periosteal origin. The periosteal blood supply is characterized by small capillaries with limited perfusion [30], which supply the osteogenic layer of the periosteum and the external surface of the cortex [31]. The distal tibia experiences alterations in the main direction of vascular flow, from centrifugal flow through medullary vessels in healthy states, to centripetal flow through periosteal capillaries in older persons with vascular disease [30–34]. This compensatory action by periosteal capillaries [30] brings essential nutrients to at-risk periosteal and midcortical bone. The presence of sub-periosteal circumferential pores may be the result of angiogenesis from a periosteal source into the cortical space, possibly as a response to hypoxia in mid-cortical regions.

The finding of adipocytes within pores located near the periosteal border was unexpected. Previous work by our group also suggested the presence of adipocytes within distal tibia cortical bone pores [35,36]; however, those previous in vivo imaging studies found adipocytes in pores located close to the endosteal border and assumed their origin to be medullary. Observations based on two-dimensional histological and three-dimensional HR-pQCT data could not confirm that the adipocyte-filled circumferential pores described in this work are physically connected to the marrow space. It is possible that these adipocytes may originate from non-medullary sources, but higher resolution 3D analysis or cellular/molecular techniques would have to be employed to explore this possibility. The high vessel density of the periosteum leads to an abundance of endothelial pericyte cells, which have the ability to differentiate into several cells types, including adipocytes [37,38]. Perivascular adipocyte progenitors could be one potential source for the adipocytes seen in the sub-periosteal circumferential pores. It is conceivable that a failed attempt to promote angiogenesis and vessel infiltration through the periosteal border, as described above, could have resulted in resorbed pores in-filled with adipocytes via pericyte differentiation.

The sites of bone matrix disintegration adjacent to the periosteal border and the sub-periosteal circumferential pores were unique to specimens from donors with both CVD and T2D. Due to the presence of small vessels, capillaries, and viable osteocytes in nearby pores and lacunae, it seems unlikely that these foci of matrix disintegration are caused by necrosis. Instead, they may be evidence of abnormal or increased perilacunar-canalicular remodeling [26,39]. Ongoing studies will evaluate the lacunocanalicular network (LCN) proximate to these zones of matrix disintegration to determine whether degeneration of the LCN secondary to compromised osteocyte function [40] may be associated with the matrix disintegration reported in these specimens.

Biomechanically, the location and size of the circumferential pores at the periosteal cortex could be detrimental to bone strength. The further pores are from the neutral axis of the long bone, the higher the bending stresses and strains experienced in the tissue surrounding the pore site during skeletal locomotion [41]. A portion of the pores documented in this work are so narrow – or wider but so close to the periosteal border – that they cannot be resolved by HR-pQCT; these may have negligible effects on bone strength. However, other pores are larger and penetrate further into the cortex, and thus can potentially impact bone

mechanics. Microindentation tests that assess bone strength at the bone surface [42] should consider that the periosteal surface of the distal tibia may be susceptible to disease and matrix deterioration, and specifically that large sub-periosteal pores may impact test results.

There are several limitations to this exploratory study. First, our sample size was small and did not include healthy controls. Further, the donors had a variety of comorbidities in addition to T2D and CVD, some of which may have skeletal sequelae. Nevertheless, the pathological features described here were common across all specimens. Second, because of the need to compare HR-pQCT images to histology, we could not perform this work in living patients and therefore have not confirmed that all features described in this manuscript can be visualized during in vivo scanning, which is subject to motion and other artifacts not present in our cadaver acquisitions. However, on retrospective analysis of existing in vivo images, we have been able to identify sub-periosteal circumferential pores that were excluded on standard analysis. Third, our specimen processing protocol did not include immunohistochemistry, which would aid in the positive identification and precise quantification of bone cells, adipocytes, and vessel structures. Finally, we have not performed rigorous quantification of the morphological features of the circumferential pores described in this study. Rather than quantifying these features from digitized histological images, which would provide adequate 2D data but incomplete 3D (axial) data, we plan to analyze pore features in 3D via HR-pQCT analysis. This technique requires extensive image processing development, which is ongoing and beyond the scope of the current publication. The observations presented here will guide this technical development, enabling HR-pQCT to provide more complete characterization of cortical microstructure and supporting future studies in larger, in vivo cohorts.

In summary, we have presented morphological pathologies affecting cortical bone in individuals with CVD and T2D. Histologically, we observed large, sub-periosteal, adipocyte-filled pores running circumferentially along the outer cortex, along with large sections of irregular, non-lamellar periosteal cortical boundary. Additionally, in sections from individuals with both T2D and CVD but not from those with CVD alone, we observed foci of periosteal bone matrix deterioration. Further, we documented that a subset of the large, sub-periosteal circumferential pores are detectable in HR-pQCT images, but have not been previously identified, likely due to limited spatial resolution, limitations of automated image processing, or lack of coordinated histological analysis. The location and content of the sub-periosteal pores emphasize the relevance of the periosteum as an alternate conduit for bone vascularization. To our knowledge, these observations have not been documented previously, and may provide insight into mechanisms of degradation of periosteal cortical bone with age and disease.

Acknowledgements

The authors thank Aaron Fields, PhD for assistance with specimen processing, Tamara Alliston, PhD for helpful discussions, and the UCSF Department of Radiology and Biomedical Imaging Research Initiative to promote Diversity in Radiology (RIDR) Program for supporting our summer student researchers.

Grant support

NIH NIAMS K01 AR056734 (GJK); NIH NIAMS R03 AR064004 (GJK); NIH NIAMS R01 AR069670 (GJK); NIH NIAMS P30 AR075055 (GJK)

References

[1]. Kazakia GJ, Tjong W, Nirody JA, Burghardt AJ, Carballido-Gamio J, Patsch JM, Link T, Feeley BT, Benjamin Ma C. The influence of disuse on bone microstructure and mechanics assessed by HR-pQCT. Bone 2014;63:132–40. 10.1016/j.bone.2014.02.014. [PubMed: 24603002]

[2]. Burt LA, Manske SL, Hanley DA, Boyd SK. Lower bone density, impaired microarchitecture, and strength predict future fragility fracture in postmenopausal women: 5-year follow-up of the calgary CaMos cohort. J Bone Miner Res 2018;33: 589–97. 10.1002/jbmr.3347. [PubMed: 29363165]

[3]. Samelson EJ, Demissie S, Cupples LA, Zhang X, Xu H, Liu C-T, Boyd SK, McLean RR, Broe KE, Kiel DP, Bouxsein ML. Diabetes and deficits in cortical bone density, microarchitecture, and bone size: framingham HR-pQCT study. J Bone Miner Res 2018;33:54–62. 10.1002/jbmr.3240. [PubMed: 28929525]

[4]. Schwartz AV. Epidemiology of fractures in type 2 diabetes. Bone 2016;82:2–8. 10.1016/j.bone.2015.05.032. [PubMed: 26027505]

[5]. Burghardt AJ, Issever AS, Schwartz AV, Davis KA, Masharani U, Majumdar S, Link TM. High-resolution peripheral quantitative computed tomographic imaging of cortical and trabecular bone microarchitecture in patients with type 2 diabetes mellitus. J Clin Endocrinol Metab 2010;95:5045–55. 10.1210/jc.2010-0226. [PubMed: 20719835]

[6]. Paccou J, Ward KA, Jameson KA, Dennison EM, Cooper C, Edwards MH. Bone microarchitecture in men and women with diabetes: The importance of cortical porosity. Calcif Tissue Int 2016;98(5):465–73. 10.1007/s00223-015-0100-8. [PubMed: 26686695]

[7]. Patsch JM, Burghardt AJ, Yap SP, Baum T, Schwartz AV, Joseph GB, Link TM. Increased cortical porosity in type 2 diabetic postmenopausal women with fragility fractures. J Bone Miner Res 2013;28:313–24. 10.1002/jbmr.1763. [PubMed: 22991256]

[8]. Shanbhogue VV, Hansen S, Frost M, Jørgensen NR, Hermann AP, Henriksen JE, Brixen K. Compromised cortical bone compartment in type 2 diabetes mellitus patients with microvascular disease. Eur J Endocrinol 2016;174:115–24. 10.1530/EJE-15-0860. [PubMed: 26537860]

[9]. Patsch JM, Zulliger MA, Vilayphou N, Samelson EJ, Cejka D, Diarra D, Berzaczy G, Burghardt AJ, Link TM, Weber M, Loewe C. Quantification of lower leg arterial calcifications by high-resolution peripheral quantitative computed tomography. Bone 2014;58:42–7. 10.1016/j.bone.2013.08.006. [PubMed: 23954758]

[10]. Paccou J, Edwards MH, Ward KA, Jameson KA, Moss CL, Harvey NC, Dennison EM, Cooper C. Ischemic heart disease is associated with lower cortical volumetric bone mineral density of distal radius. Osteoporos Int 2015;26:1893–901. 10.1007/s00198-015-3132-z. [PubMed: 25906240]

[11]. Paccou J, Edwards MH, Patsch JM, Jameson KA, Ward KA, Moss C, Dennison EM, Cooper C. Lower leg arterial calcification assessed by high-resolution peripheral quantitative computed tomography is associated with bone microstructure abnormalities in women, Osteoporos. Bar Int 2016;27:3279–87. 10.1007/s00198-016-3660-1.

[12]. Nalla RK, Kruzic JJ, Kinney JH, Ritchie RO. Effect of aging on the toughness of human cortical bone: evaluation by R-curves. Bone 2004;35:1240–6. 10.1016/j.bone.2004.07.016. [PubMed: 15589205]

[13]. Lane NE, Yao W, Balooch M, Nalla RK, Balooch G, Habelitz S, Kinney JH, Bonewald LF. Glucocorticoid-treated mice have localized changes in trabecular bone material properties and osteocyte lacunar size that are not observed in placebo-treated or estrogen-deficient mice. J Bone Miner Res 2006;21:466–76. 10.1359/JBMR.051103. [PubMed: 16491295]

[14]. Dole NS, Mazur CM, Acevedo C, Lopez JP, Monteiro DA, Fowler TW, Gludovatz B, Walsh F, Regan JN, Messina S, Evans DS, Lang TF, Zhang B, Ritchie RO, Mohammad KS, Alliston

T. Osteocyte-intrinsic TGF-β signaling regulates bone quality through perilacunar/canalicular remodeling. Cell Rep 2017;21:2585–96. 10.1016/j.celrep.2017.10.115. [PubMed: 29186693]

[15]. Tjong W, Kazakia GJ, Burghardt AJ, Majumdar S. The effect of voxel size on high-resolution peripheral computed tomography measurements of trabecular and cortical bone microstructure. Med Phys 2012;39:1893–903. 10.1118/1.3689813. [PubMed: 22482611]

[16]. Burghardt AJ, Buie HR, Laib A, Majumdar S, Boyd SK. Reproducibility of direct quantitative measures of cortical bone microarchitecture of the distal radius and tibia by HR-pQCT. Bone 2010;47:519–28. 10.1016/j.bone.2010.05.034. [PubMed: 20561906]

[17]. Buie HR, Campbell GM, Klinck RJ, MacNeil JA, Boyd SK. Automatic segmentation of cortical and trabecular compartments based on a dual threshold technique for in vivo micro-CT bone analysis. Bone 2007;41:505–15. 10.1016/j.bone.2007.07.007. [PubMed: 17693147]

[18]. Tjong W, Nirody J, Burghardt AJ, Carballido-Gamio J, Kazakia GJ. Structural analysis of cortical porosity applied to HR-pQCT data: HR-pQCT structural analysis of cortical porosity. Med Phys 2013;41:013701. 10.1118/1.4851575.

[19]. Heilmeier U, Cheng K, Pasco C, Parrish R, Nirody J, Patsch JM, Zhang CA, Joseph GB, Burghardt AJ, Schwartz AV, Link TM, Kazakia G. Cortical bone laminar analysis reveals increased midcortical and periosteal porosity in type 2 diabetic postmenopausal women with history of fragility fractures compared to fracture-free diabetics. Osteoporos. Int. J. Establ. Result Coop. Eur. Found. Osteoporos. Natl. Osteoporos. Found. USA 2016;27:2791–802. 10.1007/s00198-016-3614-7.

[20]. Nirody JA, Cheng KP, Parrish RM, Burghardt AJ, Majumdar S, Link TM, Kazakia GJ. Spatial distribution of intracortical porosity varies across age and sex. Bone 2015; 75:88–95. 10.1016/j.bone.2015.02.006. [PubMed: 25701139]

[21]. Sundh D, Nilsson M, Zoulakis M, Pasco C, Yilmaz M, Kazakia GJ, Hellgren M, Lorentzon M. High-impact mechanical loading increases bone material strength in postmenopausal women—a 3-month intervention study. J Bone Miner Res 2018;33: 1242–51. 10.1002/jbmr.3431. [PubMed: 29578618]

[22]. Moreira CA, Dempster DW. Bone histomorphometry in diabetes mellitus. Osteoporos Int 2015;26:2559–60. 10.1007/s00198-015-3258-z. [PubMed: 26243361]

[23]. Shanbhogue VV, Mitchell DM, Rosen CJ, Bouxsein ML. Type 2 diabetes and the skeleton: new insights into sweet bones. Lancet Diabetes Endocrinol 2016;4: 159–73. 10.1016/S2213-8587(15)00283-1. [PubMed: 26365605]

[24]. Napoli N, Chandran M, Pierroz DD, Abrahamsen B, Schwartz AV, Ferrari SL. Mechanisms of diabetes mellitus-induced bone fragility. Nat Rev Endocrinol 2017; 13:208–19. 10.1038/nrendo.2016.153. [PubMed: 27658727]

[25]. Willett TL, Dapaah DY, Uppuganti S, Granke M, Nyman JS. Bone collagen network integrity and transverse fracture toughness of human cortical bone. Bone 2019;120: 187–93. 10.1016/j.bone.2018.10.024. [PubMed: 30394355]

[26]. Nango N, Kubota S, Hasegawa T, Yashiro W, Momose A, Matsuo K. Osteocyte-directed bone demineralization along canaliculi. Bone 2016;84:279–88. 10.1016/j.bone.2015.12.006. [PubMed: 26709236]

[27]. Jilka RL, O'Brien CA. The role of osteocytes in age-related bone loss. Curr Osteoporos Rep 2016;14:16–25. 10.1007/s11914-016-0297-0. [PubMed: 26909563]

[28]. Seeman E Periosteal bone formation — a neglected determinant of bone strength. N Engl J Med 2003;349:320–3. 10.1056/NEJMp038101. [PubMed: 12878736]

[29]. Christen P, Müller R. In vivo visualisation and quantification of bone resorption and bone formation from time-lapse imaging. Curr Osteoporos Rep 2017;15:311–7. 10.1007/s11914-017-0372-1. [PubMed: 28639146]

[30]. Brookes M The vascular reaction OF tubular bone to ischaemia IN peripheral occlusive vascular disease. 1960. https://online.boneandjoint.org.uk/doi/pdf/10.1302/0301-620X.42B1.110. [Accessed 23 January 2020].

[31]. Cowin SC, Cardoso L. Blood and Interstitial flow in the hierarchical pore space architecture of bone tissue. J Biomech 2015;48:842–54. 10.1016/j.jbiomech.2014.12.013. [PubMed: 25666410]

[32]. Thompson B, Towler DA. Arterial calcification and bone physiology: role of the bone–vascular axis. Nat Rev Endocrinol 2012;8:529–43. 10.1038/nrendo.2012.36. [PubMed: 22473330]

[33]. Fajardo RJ. Is diabetic skeletal fragility associated with microvascular complications in bone? Curr Osteoporos Rep 2017;15:1–8. 10.1007/s11914-017-0341-8. [PubMed: 28110469]

[34]. Prisby RD. Mechanical, hormonal and metabolic influences on blood vessels, blood flow and bone. J Endocrinol 2017;235:R77–100. 10.1530/JOE-16-0666. [PubMed: 28814440]

[35]. Goldenstein J, Kazakia G, Majumdar S. In vivo evaluation of the presence of bone marrow in cortical porosity in postmenopausal osteopenic women. Ann Biomed Eng 2010;38:235–46. 10.1007/s10439-009-9850-7. [PubMed: 19953321]

[36]. Wu P-H, Gibbons M, Foreman SC, Carballido-Gamio J, Han M, Krug R, Liu J, Link TM, Kazakia GJ. Cortical bone vessel identification and quantification on contrast-enhanced MR images. Quant Imag Med Surg 2019;9:928–41.

[37]. Birbrair A, Zhang T, Wang Z-M, Messi ML, Mintz A, Delbono O. Pericytes at the intersection between tissue regeneration and pathology: Clin Sci 2015;128:81–93. 10.1042/CS20140278.

[38]. Cai X, Lin Y, Hauschka PV, Grottkau BE. Adipose stem cells originate from perivascular cells. Biol Cell 2011;103:435–47. 10.1042/BC20110033. [PubMed: 21679159]

[39]. Fowler TW, Acevedo C, Mazur CM, Hall-Glenn F, Fields AJ, Bale HA, Ritchie RO, Lotz JC, Vail TP, Alliston T. Glucocorticoid suppression of osteocyte perilacunar remodeling is associated with subchondral bone degeneration in osteonecrosis. Sci Rep 2017;7:44618. 10.1038/srep44618. [PubMed: 28327602]

[40]. Yee CS, Schurman CA, White CR, Alliston T. Investigating osteocytic perilacunar/canalicular remodeling. Curr Osteoporos Rep 2019;17:157–68. 10.1007/s11914-019-00514-0. [PubMed: 31227998]

[41]. Burr DB. Cortical bone: a target for fracture prevention? Lancet 2010;375:1672–3. 10.1016/S0140-6736(10)60444-8. [PubMed: 20472154]

[42]. Farr JN, Drake MT, Amin S, Melton LJ, McCready LK, Khosla S. In vivo assessment of bone quality in postmenopausal women with type 2 diabetes: bone quality IN women with T2D. J Bone Miner Res 2014;29:787–95. 10.1002/jbmr.2106. [PubMed: 24123088]

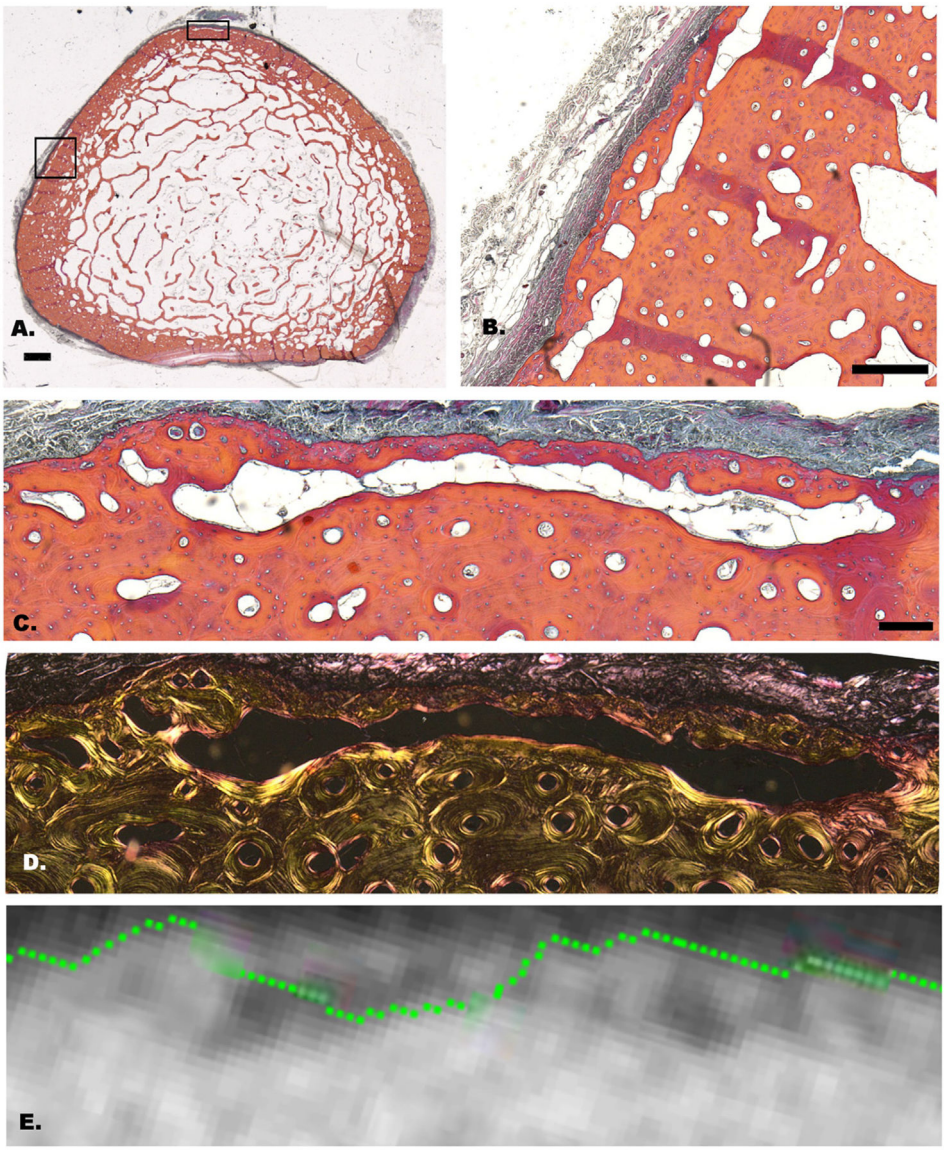

Fig. 1.

Sub-periosteal circumferential pores were observed in all sections evaluated. (A) Complete cross-section from the tibia of a patient with CVD and T2D. Black boxes indicate circumferential pores visualized in higher magnification panels (B, C). (D) Polarized light microscopy shows short, disorganized collagen fibers surrounding the circumferential pore at the periosteal border. (E) HR-pQCT image at 41 μm nominal resolution with automatically generated periosteal contour in green demonstrates that a portion of this pore would be excluded from HR-pQCT microstructural analysis. Scale bars represent 2.5 mm for (A), 500 μm for (B), and 200 μm for (C, D, E).

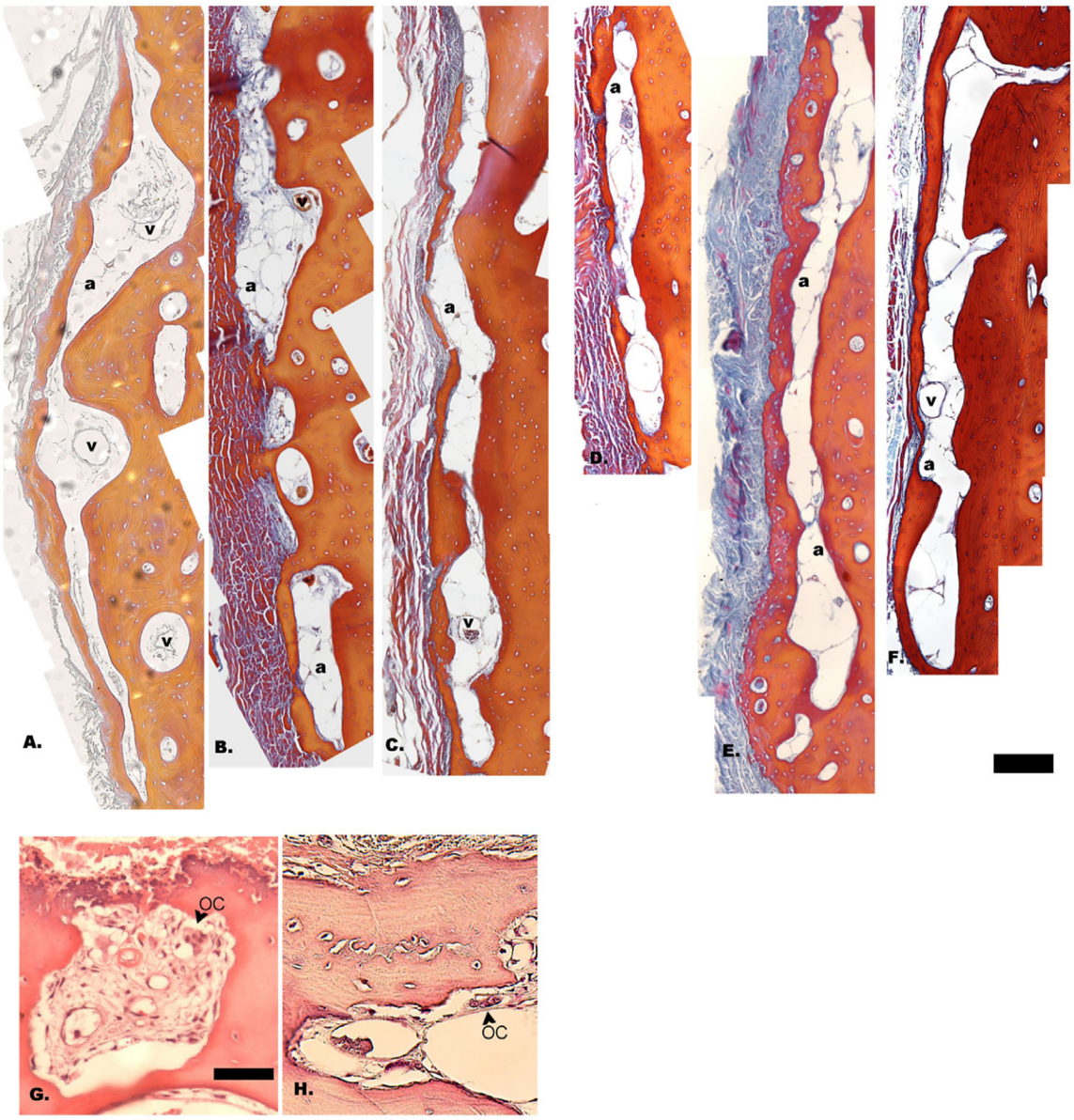

Fig. 2.

Sub-periosteal circumferential pores from each of 6 donor tibia samples. (A, B, C) Histological sections from three donors with CVD. (D, E, F) Histological sections from three individuals with both CVD and T2D. All circumferential pores detected were filled primarily with adipocytes (a); vessels (v) were denoted when present. (G, H) Osteoclasts (OC) were present within circumferential pores. Scale bars represent 200 μm for (A–F) and 50 μm for (G–H).

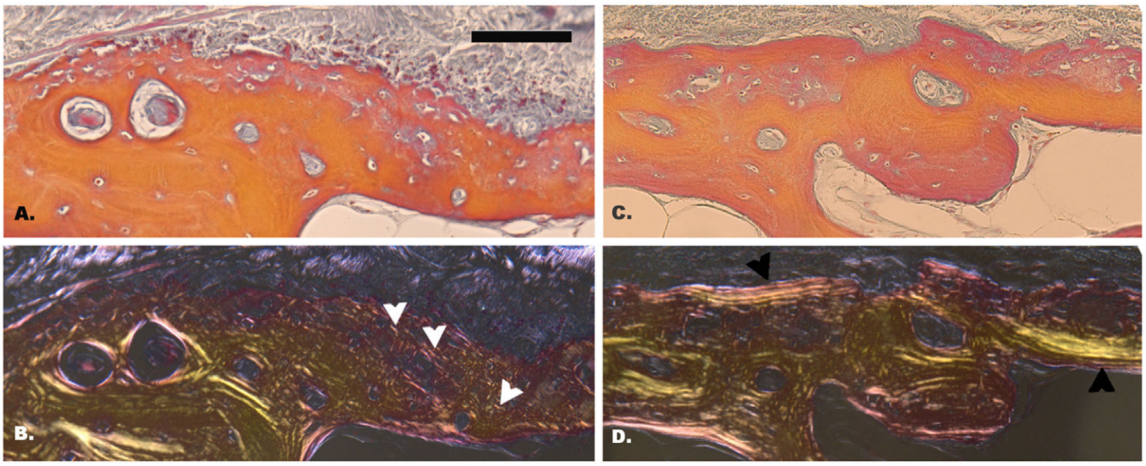

Fig. 3.

Bright field (A, C) and polarized light (B, D) microscopy of sections taken from 2 different donors shows large areas composed of short, disorganized fibers (white arrows) interspersed with organized circumferential lamellae (black arrows) at the periosteal border of the cortex. Viable osteocytes are visible within and surrounding matrix deterioration sites. Scale bar represents 100 μm.

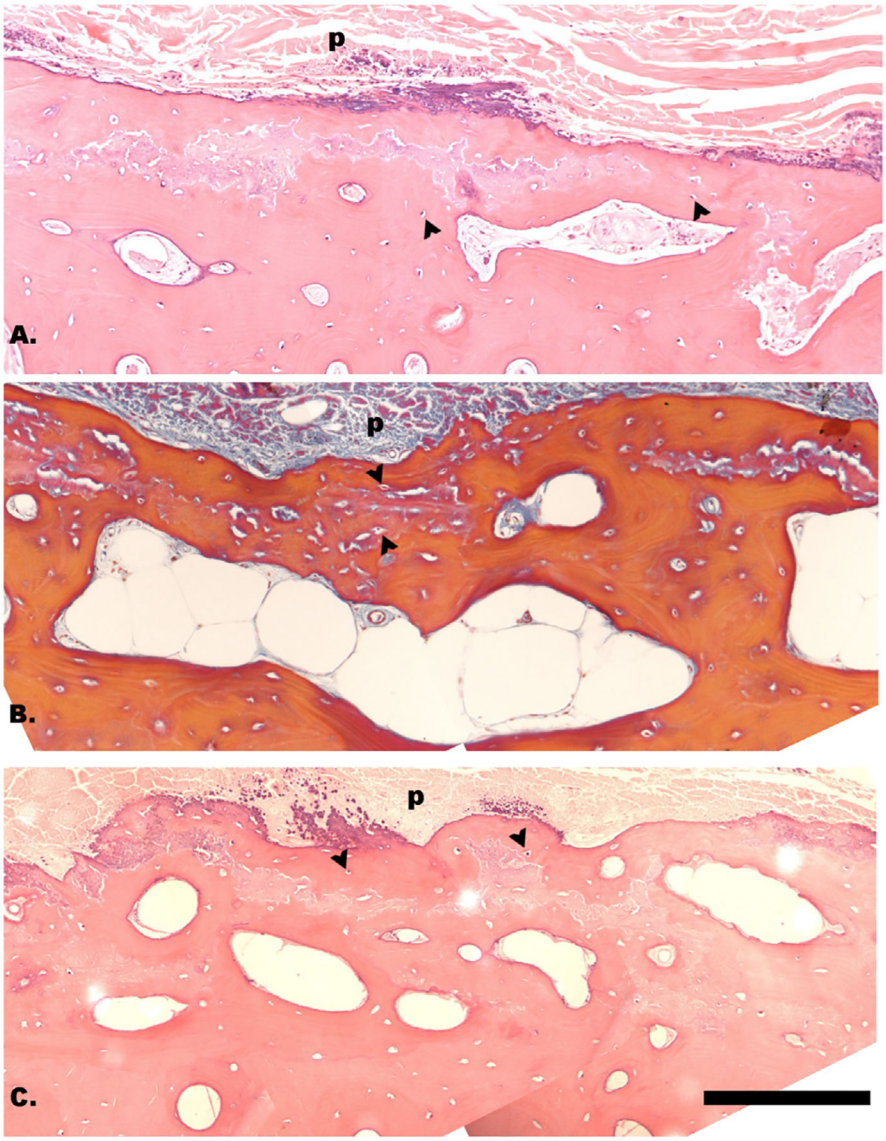

Fig. 4.

Foci of bone matrix deterioration were observed near the periosteal border in sections from donors with both CVD and T2D (A, B, C). Black arrowheads denote representative viable osteocytes in lacunae. The periosteum (p) is at the top of each of the panels. Scale bar represents 200 μm.

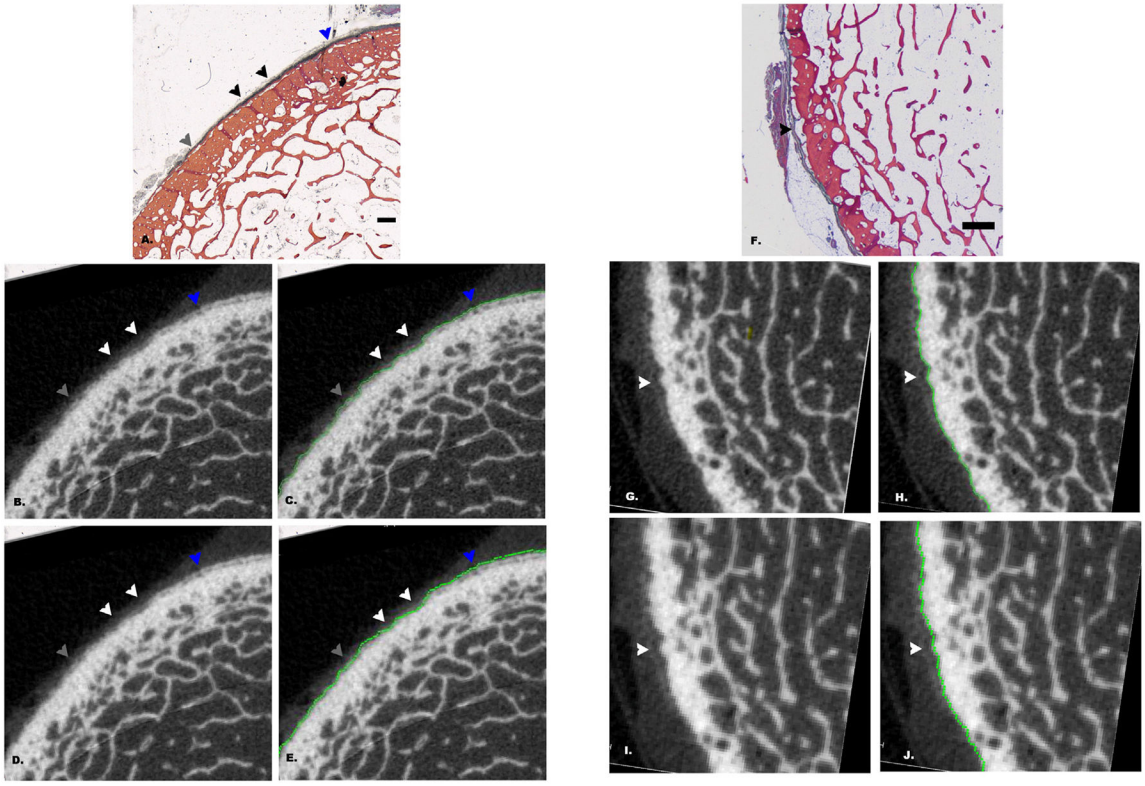

Fig. 5.

Comparison of matched HR-pQCT and histological images from 2 donor tibia samples. Sub-periosteal circumferential pores are visible on histology (A, F); circumferential pores can be detected both within 100 μm of the periosteal border (black and grey arrows) and further from the border (blue arrow). HR-pQCT images reconstructed at 41 μm (B–C, G-H) and 82 μm (D-E, I-J) are shown for comparison. Green lines represent periosteal contours created using the HR-pQCT automated image processing software. The blue arrow (A–E) indicates circumferential pores that are detectable at both 41 μm and 82 μm nominal resolutions. The white arrow pair (B–E) indicate circumferential pores that are not detected at either 41 μm or 82 μm. The single grey arrow (A–E) shows a circumferential pore that is detectable at 41 μm, but not at 82 μm nominal resolution. The single arrow (F–I) indicates a circumferential pore surrounded by a thin section of bone matrix that is undetectable at either 41 μm or 82 μm. Scale bars represent 2 mm.

Table 1

Donor characteristics. Three donors had cardiovascular disease (CVD) and three had both CVD and type 2 diabetes mellitus (T2D).

Specimen	Sex	Age (yrs.)	Disease	T2D duration (yrs.)	Fragility fractures	Comorbidities
1	female	91	CVD	NA	hip fracture	chronic kidney disease, breast cancer, arthritis
2	male	84	CVD	NA	hip fracture	chronic obstructive pulmonary disease, lung cancer
3	female	75	CVD	NA	foot and wrist fracture	skin cancer, Alzheimer's
4	male	79	CVD + T2D	10	no	lung cancer, HIV, seizures
5	female	64	CVD + T2D	20	no	pneumonia, chronic obstructive pulmonary disease
6	male	80	CVD + T2D	21	no	arthritis, skin cancer, renal infection, neuropathy